

Interacting Influence of Log Jams and Branching Channels on Hyporheic Exchange
Revealed through Laboratory Flume and Numerical Modeling Experiments

Thesis

Presented in Partial Fulfillment of the Requirements for the Degree Master of Science in
the Graduate School of The Ohio State University

By

Karl John Wilhelmsen

Graduate Program in Earth Sciences

The Ohio State University

2021

Thesis Committee

Dr. Audrey Sawyer, Advisor

Dr. Michael Durand

Dr. Joachim Moortgat

Copyrighted by
Karl John Wilhelmsen
2021

Abstract

Log jams are natural features in mountain streams that promote stream-groundwater interactions, or hyporheic exchange, through a variety of mechanisms. Log jams alter gradients in hydraulic head, increase the area available for exchange by creating backwater areas, and lead to the formation of branching channels and bars that drive additional exchange. Here, I numerically simulated stream-groundwater interactions for two constructed flume systems—one without jams and one with a series of three jams—to understand the effects of interacting jam and channel structures on hyporheic exchange. Jams increased stream-groundwater connectivity, or decreased the turnover length that stream water travels before it enters the hyporheic zone, by an order of magnitude and drove long flow paths that connected multiple jams and channel threads. The increased turnover of stream water through the bed was due mainly to the increase in the average hyporheic exchange rate, though the wetted surface area available for exchange also increased slightly. Jams with larger volumes had longer hyporheic residence times and path lengths that exhibited multiple scales of exchange. Additionally, the longest flow paths connecting multiple jams occurred in the reach with multiple channel branches. These findings suggest that large gains in hydrologic connectivity can be achieved by promoting in-stream wood accumulation and the natural formation of both jams and branching channels.

Acknowledgments

This work was supported by funding from the National Science Foundation under award number EAR-1819086. Funds were also provided by the Geological Society of America through a Graduate Student Research Grant. I would like to thank Anna Marshall and Sawyer McFadden as project colleagues and for their work constructing and operating our experimental flume. I thank Dr. Kamini Singha and Dr. Ellen Wohl for their support as mentors and teachers in the execution of this research project. I thank Jacob Clyne for his dedicated assistance in field data collection and invaluable support both in working through research concepts and as a laboratory colleague. I thank my committee members, Dr. Michael Durand and Dr. Joachim Moortgat, for their guidance and insights throughout this project. I would also like to thank my advisor, Dr. Audrey Sawyer, for her work as my mentor and guiding me as I developed my skills conducting hydrogeology research.

Vita

- 2015 B.S. Environmental Resources Engineering, SUNY College of
 Environmental Science and Forestry
- 2015-2019 Associate Engineer, FPM Remediations, Inc.
- 2019-present Graduate Research and Teaching Associate, School of Earth Sciences, The
 Ohio State University

Fields of Study

Major Field: Earth Sciences

Table of Contents

Acknowledgments.....	iii
Vita.....	iv
List of Tables	vi
List of Figures	vii
Chapter 1. Introduction	1
Chapter 2. Methods.....	5
2.1 Flume Setup	5
2.2 Numerical Modeling	8
2.3 Model Assessment	11
Chapter 3. Results	18
3.1 Effect of Jam Structures on Exchange Rates and Connectivity	18
3.2 Complexities in Hyporheic Flow Paths and Residence Times	20
Chapter 4. Discussion	26
4.1 Jam Structures Drive Hyporheic Flow and Chemical Reaction Potential in the Hyporheic Zone	26
4.2 Multiple Channel Threads and Big Jams Increase Hyporheic Interactions	30
Chapter 5. Conclusion.....	32
Bibliography	33
Appendix A. Model Development and HydroGeoSphere Input Files	39

List of Tables

Table 1. Definition of parameters and values for simulations.	13
Table 2. Trial runs to constrain less well-known parameters	15

List of Figures

Figure 1. Physical flume experiment and model simulation domain.....	6
Figure 2. Aerial image of flume structure and digital elevation model	7
Figure 3. Model-data agreement below Jam 1	16
Figure 4. Model-data agreement below Jam 3	17
Figure 5. Hyporheic exchange flux maps across the wetted streambed	19
Figure 6. Flow paths across Jam 1 for medium discharge	21
Figure 7. Flow paths across Jams 2 and 3 for the medium stream discharge	21
Figure 8. Flux weighted distributions of hyporheic flow path lengths across each jam structure.....	22
Figure 9. Hyporheic path length as a function of jam volume.....	23
Figure 10. Flux weighted distributions of hyporheic residence times across each jam structure.....	24
Figure 11. Reach-scale hyporheic path length distributions	25
Figure 12. Reach-scale hyporheic residence time distributions.....	25
Figure 13: Reaction significance factor per km as a function of stream flow rate	29

Chapter 1. Introduction

Hyporheic exchange, or mixing between streams and groundwater, is driven by hydraulic head gradients along the streambed, which occur where currents interact with ripples and pool-riffle sequences (Gooseff et al., 2006; Buffington & Tonina, 2009), channel bends (Wondzell et al., 2009), and large wood jams (Tonina & Buffington, 2009; Beckman & Wohl, 2014). The benefits of hyporheic exchange are diverse, including nutrient retention (Valett et al., 1997; Crenshaw et al., 2002; Harvey et al., 2013), pollutant degradation (Gandy et al., 2007), buffering of surface water and streambed temperatures (Arrigoni et al., 2008; Majerova et al., 2015), and improvement of aquatic habitat (Hester and Gooseff, 2010; Xu et al., 2012). For example, hyporheic exchange supplies oxygen to shallow sediments where fish embryos and macroinvertebrates dwell and modifies daily temperature fluctuations, impacting invertebrate diversity and hatching times of salmonid eggs (Evans & Petts, 1997).

Large wood is a natural feature in mountain streams that promotes hyporheic exchange through multiple mechanisms, both direct and indirect (Tonina & Buffington, 2009; Majerova et al., 2015). Directly, structures such as channel-spanning logs and steps increase hydraulic head gradients that drive flow through the bed (Curran & Wohl, 2003; Lautz et al., 2006; Endreny et al., 2011; Sawyer et al., 2011). Indirectly, jams also enhance step-pool and pool-riffle systems (Montgomery & Buffington, 1997; Curran &

Wohl, 2003) and force anabranching channels (Abbe & Montgomery, 1996; Sear et al., 2010), all of which promote vertical and lateral flow (Buffington & Tonina, 2009; Gooseff et al., 2006; Tonina & Buffington, 2007). Moreover, large wood increases alluvial cover in streambeds that would otherwise have exposed bedrock (Massong & Montgomery, 2000; Faustini & Jones, 2003; Montgomery et al., 2003; Buffington & Tonina, 2009), thus creating a potential region for hyporheic mixing. Under high-flow conditions, jams also retain water in upstream pools and release it from storage through surface and hyporheic flow paths under subsequent low-flow conditions (Nyssen et al., 2011). In summary, reaches with established jam structures are more likely to exhibit greater complexity in head gradients, channel morphology, and streambed sediment cover, all of which interact to enhance hyporheic flow (Sear et al., 2010; Livers & Wohl, 2016).

Due to the morphologic complexity of streams with numerous jams, it can be challenging to quantify hyporheic exchange in the field at relevant scales that span multiple jams and related channel features. Scaled flume experiments offer an alternative approach to understand the interacting effects of log jams and channel morphologic complexity on hyporheic exchange. The flume system can be controlled for substrate properties, surface water discharge, channel planform, and wood presence. Incorporating numerical models makes it possible to analyze hyporheic flow paths within flumes at greater spatial resolution than possible with observations (Savant et al., 1987; Salehin et al., 2004; Tonina & Buffington, 2007; Endreny et al., 2011). Previous studies have combined flume experiments with numerical models to analyze hyporheic exchange due

to relatively simple log-formed structures. Sawyer et al. (2011) examined single, channel-spanning logs and showed that the hyporheic exchange rate scales with the blockage ratio (fraction of channel depth obstructed by the log) and channel Froude number. Endreny et al. (2011) analyzed hydraulic jumps and hyporheic flow around steps and found that hydraulic jumps create heterogeneity in downwelling/upwelling patterns and hyporheic flow paths. They suggested these patterns likely impact the transport of redox-sensitive solutes and biogeochemical conditions within sediments. Fewer controlled flume studies have examined the effects of multiple large wood structures on hyporheic exchange. Mutz et al. (2007) ran experiments with abundant wood and found that greater wood presence alters bedforms and increases flow resistance and vertical exchange, but their flume configuration did not allow for anabranching channels, which are often observed near log jams in the field (Sear et al., 2010; Collins et al., 2012). While these flume studies have shaped our understanding of hyporheic exchange around individual structures and, to some extent, the interactions between structures, an opportunity exists to test relations between multiple jams and more complex jam-formed channel morphologies.

I integrate high-resolution coupled surface water-groundwater flow models to analyze hyporheic flow in an experimental flume with multiple jams and branching channels. The flume setup is inspired by field observations from Little Beaver Creek (Doughty et al., 2020), a 3rd-order stream in the Rocky Mountains of Colorado, USA. Related studies by Marshall et al. (in prep.) and Ader et al. (2021) detail the effects of in-stream wood on transient storage in the experimental flume and Little Beaver Creek,

respectively. Here, I show that the presence of jam structures and multithreaded channels encourages longer, multidimensional hyporheic flow paths that encompass multiple jam and channel structures. Larger jam structures play a key role in driving a more complex hyporheic regime by increasing bed exchange rates and expanding the length scales and residence times of hyporheic flows.

Chapter 2. Methods

2.1 Flume Setup

The physical flume has an experimental section that is 9.2 m long and 1.2 m wide with a sediment box that is 0.1 m deep. The overall slope is 0.01 m/m, or 1% (Figure 1). Water cascades into the experimental section over a stepped spillway. The sediment in the experimental section is generally composed of a layer of coarse sand and an armored surface layer with gravel and coarse sand. The median grain sizes of the deep layer and surface layer are 2.83 mm and 12.7 mm, respectively. According to the Shahabi empirical method (Shahabi et al., 1984; Dolzyk & Chmielewska, 2014), hydraulic conductivities are estimated as 8.89×10^{-5} m/s for the deep layer and 2.54×10^{-3} m/s for the armored surface layer, but model-data comparison, described in Section 2.3, and hydraulic characteristics of unconsolidated gravel and sand sediments (Freeze & Cherry, 1979), suggests that hydraulic conductivities are likely an order of magnitude greater. The two layers' porosities are estimated at 0.3, typical of unconsolidated fluvial sediments (Freeze & Cherry, 1979).

Three log jams were formed by hand to examine the effects of log jam and channel complexities on hyporheic exchange dynamics (Figure 1). From upstream to downstream, Jam 1 is located within a single channel and has a volume of 0.024 m^3 , as measured by the total space occupied by the wood pieces. Jam 2 spans two channel

threads and has a volume of 0.041 m^3 . Jam 3 spans two channel threads and is a more complex jam structure comprised of multiple, larger wood pieces with a total volume of 0.070 m^3 . Given the similar wood materials and construction approach for each jam, all three jams were estimated to have a porosity of 0.7, the upper limit of the expected range for large wood jams in the field (0.6 to 0.7) (Spreitzer et al., 2020).

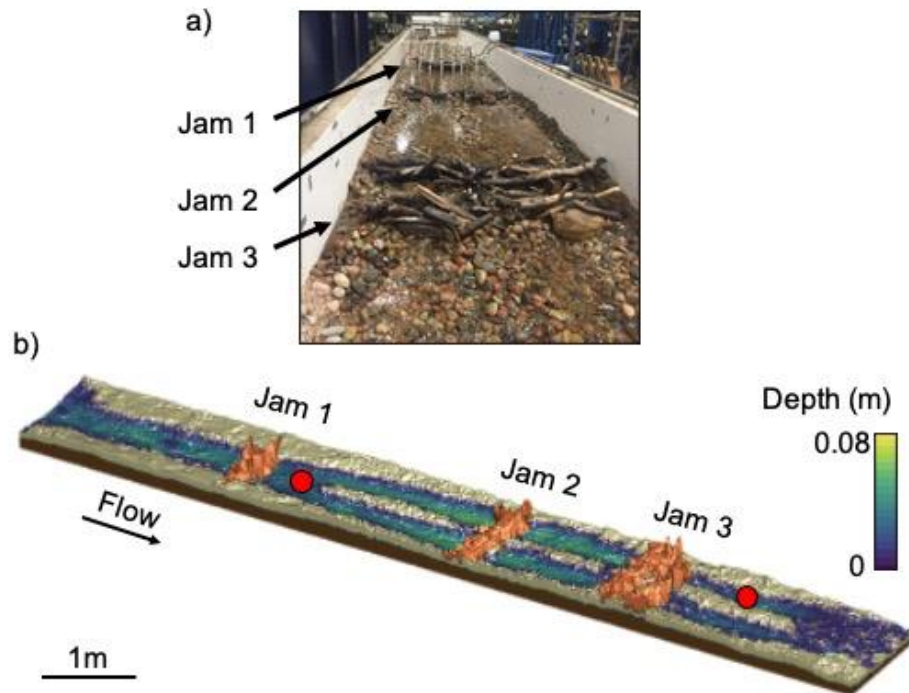


Figure 1. a) Photo of the flume looking upstream. b) Digital elevation model, draped with surface water depths simulated under a discharge of 1.42 L/s . Red circles denote locations where fluid electrical conductivity was measured in surface water within the flume and compared with numerical simulations.

Experiments were conducted under three flow conditions: low-flow (1.42 L/s), medium-flow (4.25 L/s), and high-flow (8.50 L/s). For each run, a conservative salt tracer was injected continuously for two hours, and solute breakthrough curves were monitored with conductivity sensors at multiple locations in surface water every 5.0 seconds (Figure 1b).

A digital elevation model for the flume was constructed using structure from motion. Images were captured at regular downstream intervals with a camera mounted at consistent elevation. Images were processed using Agisoft, a photogrammetry software. The resulting digital elevation model has a resolution of less than 1 mm (Figure 2). In order to compare hyporheic exchange with and without the influence of jams, the jams were removed, and the image capture process was repeated.

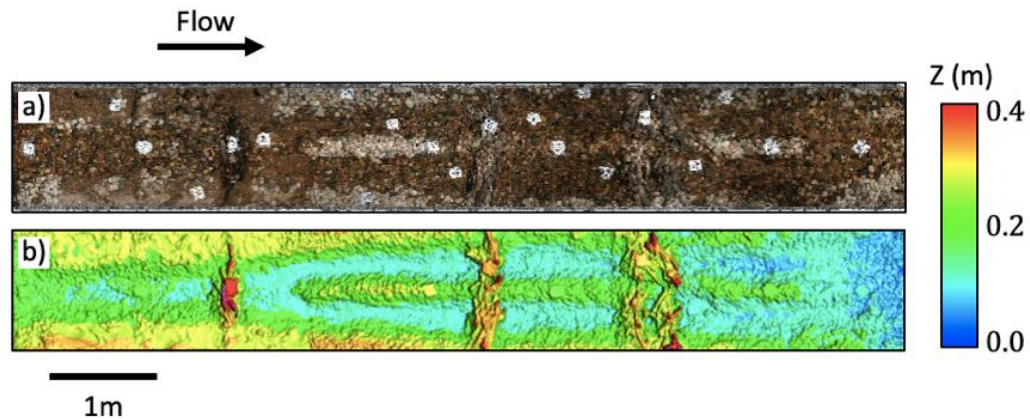


Figure 2. a) Aerial image of flume structure. b) Digital elevation model. White dots present in (a) are reference locations used in the photogrammetry processing.

2.2 Numerical Modeling

Surface water flow was represented using the shallow water equations:

$$\frac{dh}{dt} + \nabla \cdot (\bar{\mathbf{v}}d_o) + d_o\Gamma_o = 0 \quad (1)$$

$$\frac{d\bar{\mathbf{v}}}{dt} + \bar{\mathbf{v}} \cdot \nabla(\bar{\mathbf{v}}) + g\nabla d_o = g(\mathbf{S}_o - \mathbf{S}_f) \quad (2)$$

where h is the water surface elevation, d_o is the depth of flow, $\bar{\mathbf{v}}$ is the vertically-averaged flow velocity, Γ_o is the exchange rate between the surface and subsurface domains, g is the acceleration due to gravity, and S_o and S_f are the bed and friction slopes, respectively, with S_f calculated from the Manning equation. The roughness coefficient used for surface flow was 0.030, typical of gravel beds with no vegetation (Table 1) (Phillips et al., 2006). Through the interfacial exchange flux, Γ_o , Equations 1 and 2 were coupled to the three-dimensional variably saturated groundwater flow equation:

$$-\nabla \cdot (-\mathbf{K} k_r \nabla(\psi + z)) + \Gamma_o = \frac{\partial}{\partial t} (\theta_s S_w) \quad (3)$$

where \mathbf{K} is the hydraulic conductivity tensor, k_r is the relative permeability, ψ is pressure head, z is elevation head, θ_s is saturated water content (or porosity), and S_w is the degree of water saturation, θ/θ_s , where θ is water content. The relationship between water content and pressure head is controlled by the van Genuchten parameters (Table 1), which were chosen to be representative of sandy sediments (Zhu & Mohanty, 2002). In Equations 1-3, water is assumed to be incompressible with uniform density. Equations 1 and 2 ignore vertical velocity structure in recirculation zones downstream from jams, but

the primary goal of the models is to resolve subsurface flow structure, which is driven by gradients in hydraulic head, rather than the surface flow structure. The shallow water equations have been used to simulate stream-groundwater interactions for a wide variety of complex, multidimensional flows, including cases where stream flow is fully turbulent (Leclerc et al., 1990; Heniche et al., 2000; Wang et al., 2002; Chow et al., 2019). Chow et al. (2019) confirmed that Equations 1-3 adequately characterize hyporheic exchange in a turbulent river so long as the model bathymetry resolves local-scale bedforms that drive hyporheic exchange (Chow et al., 2019).

The base and sides of the model were defined as no-flow boundaries to represent the bottom and sides of the flume environment. At the upstream boundary of the flume domain, a specified inflow flux was assigned to simulate the stepped spillway. At the downstream outlet, a critical depth boundary condition was established to match flume observations. The model was initialized with an impermeable bed and run until surface water flow approached steady state. These results were used as initial conditions for a second transient simulation with a permeable bed in order to achieve steady conditions in both the surface and subsurface (Appendix A).

Simulations were run using the control volume finite element method in HydroGeoSphere (Huyakorn et al., 1986; Panday, 1993; Therrien, 1992; Therrien and Sudicky, 1996). The surface of the domain was discretized with an unstructured, triangular mesh with maximum element length of 2.0 cm. While the minimum element size is coarser than the resolution of the digital elevation model, a finer mesh would have been inconsistent with the concept of a porous continuum for the coarse sediments used

in the flume. The subsurface was discretized using two porous media domains. The deeper porous media elements were assigned element heights of 0.028 m while the three near-surface sediment layers were assigned element heights of 0.005 m. Jam structures were represented in the model as additional porous media domains that extended above the height of the surface water and acted as permeable dams. The decision to treat the jams as porous media was both precedented and practical. Field studies have previously considered jams as porous media and estimated their porosities (Spreitzer et al., 2020). Treating flow through the jams as an open-water process would have required full three-dimensional solutions to the Navier-Stokes equations. My interest was not in understanding the velocity fields within the jams but their effect on hydraulic heads and hyporheic exchange, which should be well-represented in the chosen model framework (Xu & Liu, 2017; Ventres-Pake et al., 2020). General model performance was checked by comparing a solute transport simulation with flume tracer experimental results, described in Section 2.3.

Particle tracking was used to visualize hyporheic flow paths in Tecplot and analyze hyporheic residence time distributions. Specifically, particles were released along the sediment-water interface from fully saturated model nodes with downward-directed fluid flux, and they were tracked while they remained in the sediment (jams were considered part of the surface water domain). In reach-scale residence time distributions, particles were released across the entire saturated sediment-water interface; in residence time distributions for individual jams, particles were only released from the pool upstream of each jam. Frequencies of particle residence times and path lengths were flux

weighted. The total number of particles tracked across individual jams varied between 1,096 and 3,950, while the total number of particles across the reach varied between 16,352 and 31,575, depending on runs. I did not include particles with path lengths less than 0.01 m, the approximate length scale of individual sediment grains, in our residence time or particle path distributions.

I computed additional reach-scale hyporheic metrics to compare simulations with and without jam structures, including the average hyporheic exchange rate and the turnover length. The average hyporheic exchange rate (q_{swi}) was computed by integrating the positive (upwelling) exchange fluxes across the bed and dividing by the wetted streambed area, A . The degree of hyporheic connectivity was calculated as the turnover length (L), or average distance water travels downstream before it enters the bed (Newbold et al., 1983; Harvey and Wagner, 2000):

$$L = \frac{Q}{q_{swi}A} L_f \quad (4)$$

where Q is stream discharge and L_f is the length of the flume. Turnover length is a useful metric for considering the potential impacts of hyporheic exchange on stream water quality, assuming chemical transformations predominantly occur within the streambed.

2.3 Model Assessment

In order to verify that hyporheic exchange was adequately represented using the coupled shallow-water equations and permeable jam structures, I simulated a two-hour salt tracer injection similar to one performed in the flume and compared modeled breakthrough curves with measured electrical conductivity observations. To simulate the

tracer injection, steady velocity fields and water depths from Equations 1-3 were used as inputs to the unsteady conservative solution transport equations for surface water and the porous subsurface (Bear, 1972; Jaiswal et al., 2018):

$$\nabla \cdot (\mathbf{D}_o \nabla C) - \nabla \cdot (\bar{\mathbf{v}} C) - d_o \Omega_o = \frac{\partial C}{\partial t} \quad (5)$$

$$\nabla \cdot (\mathbf{D} \nabla C) - \nabla \cdot (\mathbf{q} C) + \Omega_o = \frac{\partial \theta_s S_w C}{\partial t} \quad (6)$$

where \mathbf{D}_o and \mathbf{D} are the hydrodynamic dispersion tensors for the surface and subsurface, respectively, C is the solute concentration, \mathbf{q} is Darcy flux, and Ω_o is the mass exchange rate of solute from the surface to the subsurface domain. The hydrodynamic dispersion tensors, \mathbf{D}_o and \mathbf{D} , are:

$$\mathbf{D}_o = (\alpha_l - \alpha_t) \frac{\mathbf{v}\mathbf{v}}{|\mathbf{v}|} + \alpha_t |\mathbf{v}| \mathbf{I} + D_m \mathbf{I} \quad (7)$$

$$\mathbf{D} = \frac{(\alpha_{l,p} - \alpha_{t,p}) \frac{\mathbf{q}\mathbf{q}}{|\mathbf{q}|} + \alpha_{t,p} |\mathbf{q}|}{\theta_s S_w} + D_m \mathbf{I} \quad (8)$$

where α_l is the surface water longitudinal dispersivity, α_t is the surface water transverse dispersivity, $\alpha_{l,p}$ is the porous media longitudinal dispersivity, $\alpha_{t,p}$ is the porous media transverse dispersivity, D_m is the molecular diffusion coefficient, and \mathbf{I} is the identity matrix (Table 1). The molecular diffusion coefficient was set to the value for sodium chloride at the low concentrations achieved in the flume (Guggenheim, 1954).

Variable	Definition	Value	Units
S_w	residual saturation	0.053	-
n	Manning's coefficient	0.030	s/m ^{1/3}
θ_s	porosity (sediment)	0.30	-
	van Genuchten alpha	3.548	1/m
	van Genuchten gamma	3.162	-
α_l	longitudinal dispersivity (stream)	1.4	m
α_t	transverse dispersivity (stream)	1.4	m
$\alpha_{l,p}$	longitudinal dispersivity (sediment)	0.05	m
$\alpha_{t,p}$	transverse dispersivity (sediment)	0.005	m
D_m	molecular diffusion coefficient	1.613x10 ⁻⁹	m ² /s
$K_{shallow}$	hydraulic conductivity (upper layer)	2.54x10 ⁻²	m/s
K_{deep}	hydraulic conductivity (lower layer)	8.89x10 ⁻⁴	m/s
K_{jam}	hydraulic conductivity (jams)	1.0	m/s
θ_s	porosity (jams)	0.70	-

Table 1. Model parameters and values.

At the inlet, a specified concentration signal was assigned to match the two-hour injection in the flume. The sides and base of the model were specified as zero solute mass flux boundaries, while the downstream outlets of the surface and subsurface domains were specified as zero dispersive-flux (outflow) boundaries. Computational time steps of 5.0 s were chosen to maintain Courant numbers below 4 and Peclet numbers below 2 to control for stability and numerical dispersion (El-Kadi & Ling, 1993).

In total, 9 runs were repeated for high and low values of some of the most uncertain parameters, including sediment and jam hydraulic conductivities (K_{deep} , $K_{shallow}$, and K_{jam}) and surface and subsurface dispersivity values (α_l , $\alpha_{l,p}$) (Table 2, Figures 3 and 4). Initial testing suggested that Manning's roughness (n) and molecular diffusion (D_m) had little influence on solute transport, and these values were not modified further. Jam hydraulic conductivity (K_{jam}) had a large influence on instream backwater effects and was

tested over a relatively narrow range to maintain reasonable backwater conditions. Surface and subsurface dispersivity values ($\alpha_l, \alpha_{l,p}$) were tested over larger ranges, recognizing that dispersion can vary greatly in both laboratory experiments and natural streams (Elder, 1959; Glover, 1964; Fischer 1965; Fischer, 1968).

All simulations generally captured the overall breakthrough behavior, with rapid decline in salt concentrations within minutes after injection ended, followed by a gradual return to background concentrations over the next 30 minutes (Figures 3 and 4). However, simulations tended to overestimate the bulk travel time (when concentrations had fallen to half their maximum value) by 90-105 seconds and underestimate the longer salt travel times that contribute to a “heavy tail” in the solute breakthrough curve. I consider the general model performance here to be adequate for examining hyporheic exchange through jam structures like the ones created in the flume.

Hydraulic conductivity of the upper and lower sediment layers had a strong influence on model breakthrough curves. Trial 7 closely matched the bulk solute transport below Jam 1 (Figure 3d), while Trials 3 and 9 more closely matched the late-time behavior below Jam 3 (Figure 3a-3e). These trials all had the same hydraulic conductivities for the sediment layers and jams, and these values were therefore used in all reported model simulations (Table 1). Trials 3, 7, and 9 only differed in terms of their dispersivities in the surface and subsurface (Table 2). However, my analysis of hyporheic fluxes, path lengths, and residence times (which are advection-based) does not depend on dispersion.

	K_{deep}	$K_{shallow}$	K_{jam}	$\alpha_l = \alpha_t$	$\alpha_{l,p}$
Trial 1	8.89×10^{-4}	2.54×10^{-2}	0.8	1.4	0.05
Trial 2	8.89×10^{-4}	2.54×10^{-2}	1.2	1.4	0.05
Trial 3	8.89×10^{-4}	2.54×10^{-2}	1.0	1.4	0.05
Trial 4	8.89×10^{-5}	2.54×10^{-2}	1.0	1.4	0.05
Trial 5	8.89×10^{-4}	2.54×10^{-3}	1.0	1.4	0.05
Trial 6	8.89×10^{-4}	2.54×10^{-2}	1.0	0.7	0.05
Trial 7	8.89×10^{-4}	2.54×10^{-2}	1.0	0.14	0.05
Trial 8	8.89×10^{-4}	2.54×10^{-2}	1.0	1.4	0.01
Trial 9	8.89×10^{-4}	2.54×10^{-2}	1.0	1.4	0.10

Table 2. Trial runs to constrain less well-known parameters. Note $\alpha_{t,p} = \frac{\alpha_{l,p}}{10}$.

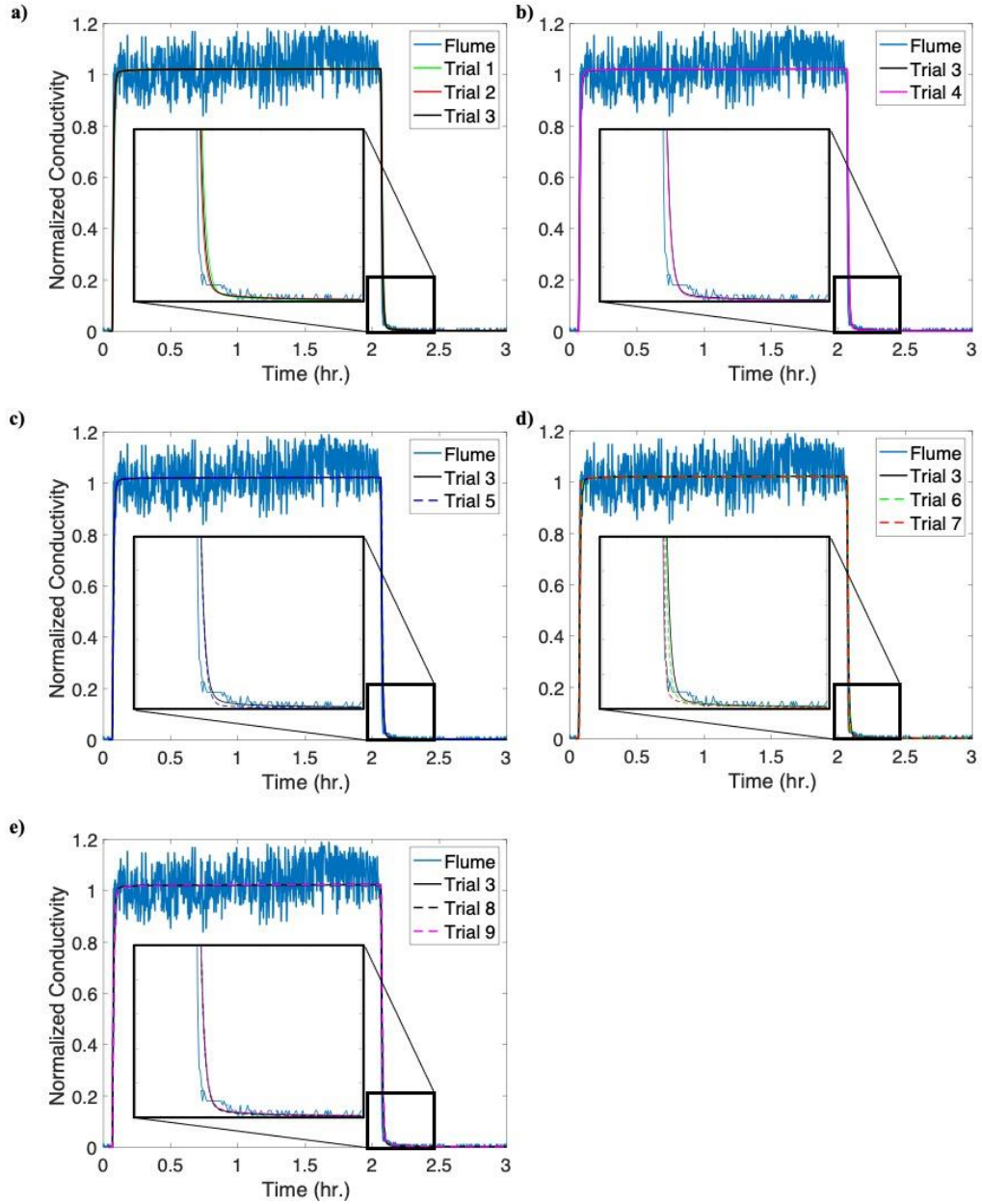


Figure 3. Model-data agreement below Jam 1 for the nine numerical simulations, described in Table 2, comparing changes in a) K_{jam} , b) K_{deep} , c) $K_{shallow}$, d) α_l and α_t , and e) $\alpha_{l,p}$ and $\alpha_{t,p}$. Electrical conductivity is normalized to more closely compare the numerical simulations to the field measurements: 1 represents peak conductivity readings and 0 represents background.

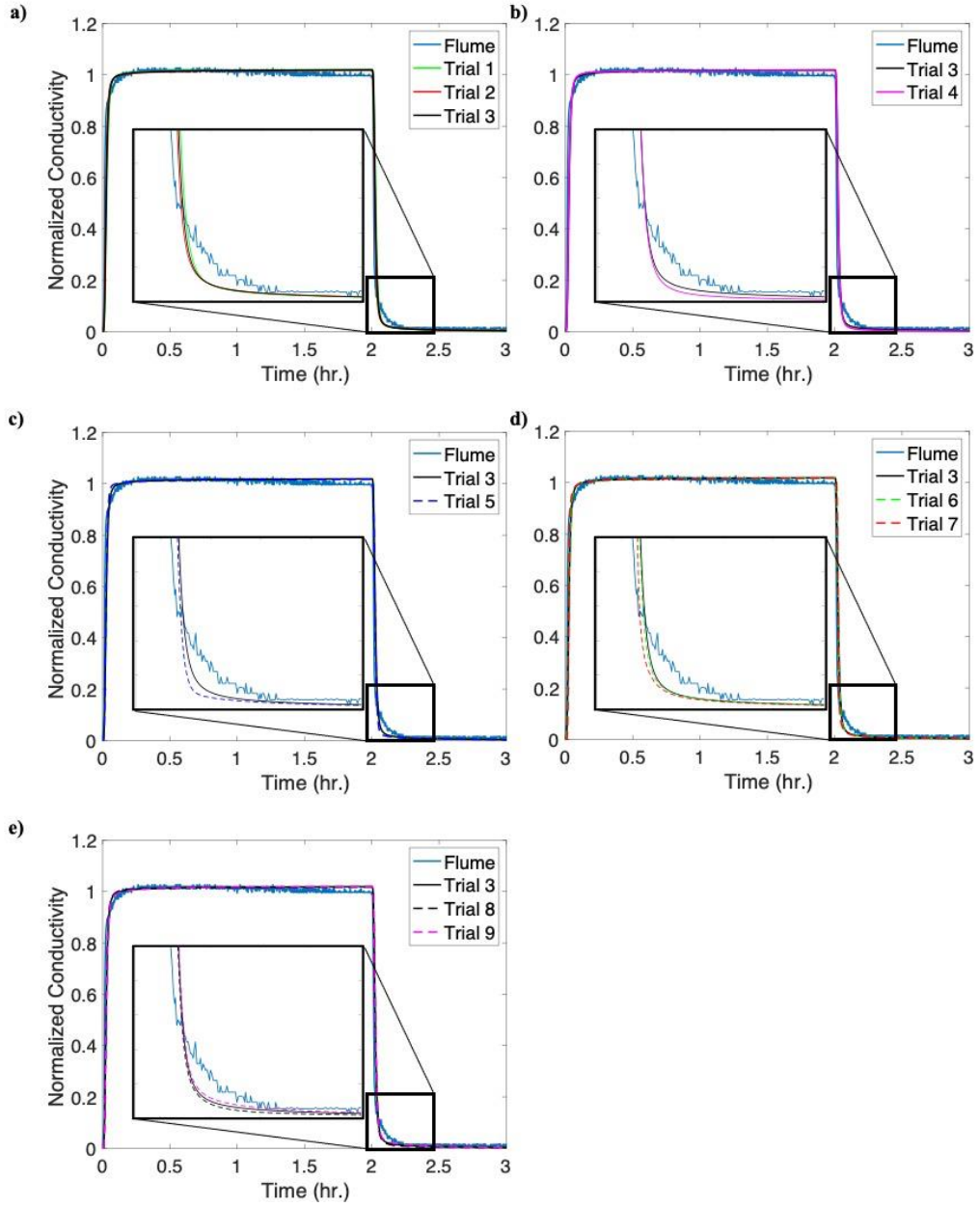


Figure 4. Model-data agreement below Jam 3 for the nine numerical simulations, described in Table 2, comparing changes in a) K_{jam} , b) K_{deep} , c) $K_{shallow}$, d) α_l and α_t , and e) $\alpha_{l,p}$ and $\alpha_{t,p}$. Electrical conductivity is normalized to compare the numerical simulations to the field measurements: 1 represents peak conductivity readings and 0 represents background.

Chapter 3. Results

3.1 Effect of Jam Structures on Exchange Rates and Connectivity

Around jam structures, downwelling characteristically occurs in the upstream pools, and upwelling occurs in the downstream channels (Figure 5). Away from jam structures, exchange patterns are dominated by short flow paths on the length scale of irregularities in the planar bed (~3-10 cm). The average hyporheic exchange rate increases with streamflow from 1.26×10^{-3} m/s to 3.48×10^{-3} m/s for stream discharge rates of 1.42 L/s to 8.50 L/s. This corresponds with observed increases in stream depth and head gradients along the sediment-water interface, particularly in the pools above the jams. For comparison, simulations without jams lack the larger-scale exchange patterns (Figure 5d, 5e, and 5f). The average exchange flux rate is far lower (2.09×10^{-4} m/s to 2.92×10^{-4} m/s) and changes little with stream discharge.

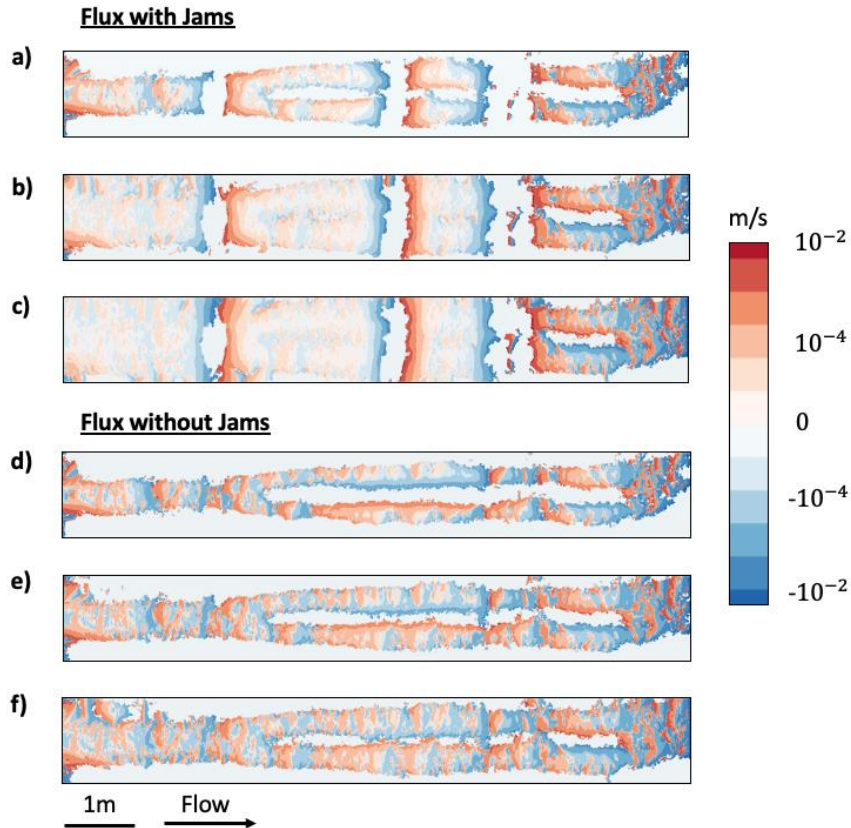


Figure 5. Hyporheic exchange flux maps across the wetted streambed for: a) low-flow, b) medium-flow, and c) high-flow conditions for the simulations with jam structures, and d) low-flow, e) medium-flow, and f) high-flow conditions for the simulations with no jam structures. Positive values indicate upwelling and negative values indicate downwelling. Note change in color bar range for simulations d, e, and f.

Jams not only increase average exchange rates but also create more area for exchange by creating backwater effects, particularly under higher stream discharge rates. Under medium and high stream flow rates, the wetted streambed area increases by 37-38%. At low-flow rates, the wetted streambed area only increases 9% with jams.

Turnover length substantially decreases in the presence of jam structures due to both changes in the area available for exchange and the flux across the bed. In the

presence of jams, the turnover lengths for the low, medium, and high stream flows are 1.83 m, 1.85 m, and 1.97 m, respectively. Without jams, the lengths are 8.62 m, 24.1 m, and 45.4 m, respectively. Only 9-38% of the differences in turnover lengths with and without jams are due to the increase in wetted streambed area (A in Equation 4), while the remainder is due to the increase in exchange flux (q_{swi} in Equation 4).

3.2 Complexities in Hyporheic Flow Paths and Residence Times

Hyporheic flow paths around jams vary depending on their position within single or multiple channel threads and also across stream flow rates. In the single channel around Jam 1, water downwells under the jam structure and upwells immediately downstream of the jam with only little interaction with the channel banks (Figure 6). However, in the multithreaded channel system, hyporheic flow paths span Jams 2 and 3 and interact with the central gravel bar (Figure 7). Some of the downwelling flow that originates in the pool upstream of Jam 2 travels through the hyporheic zone and resurfaces downstream of Jam 3 in the gravel bar separating the channels. Similarly, some of the hyporheic flow originating in the pool upstream of Jam 3 travels under the jam structure and moves laterally into the stream banks. A portion of this flow exits the subsurface at the downstream extent of the flume and would have presumably resurfaced even farther downstream if not for the finite flume length.

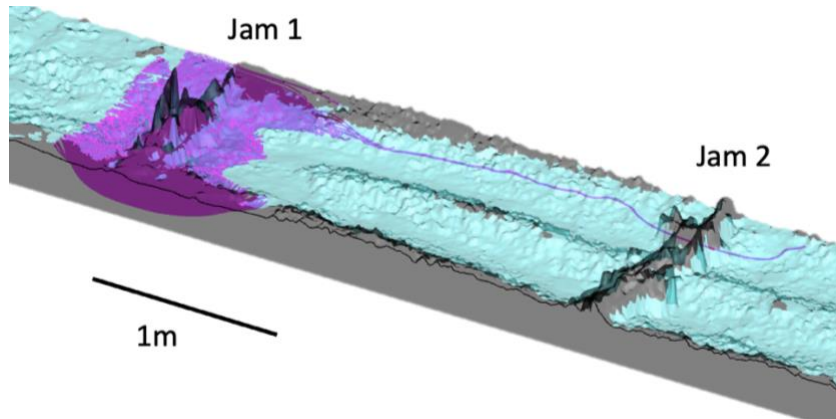


Figure 6. Flow paths (purple) across Jam 1 for medium discharge. Most downwelling flow upstream of the log jam upwells immediately downstream of the structure.

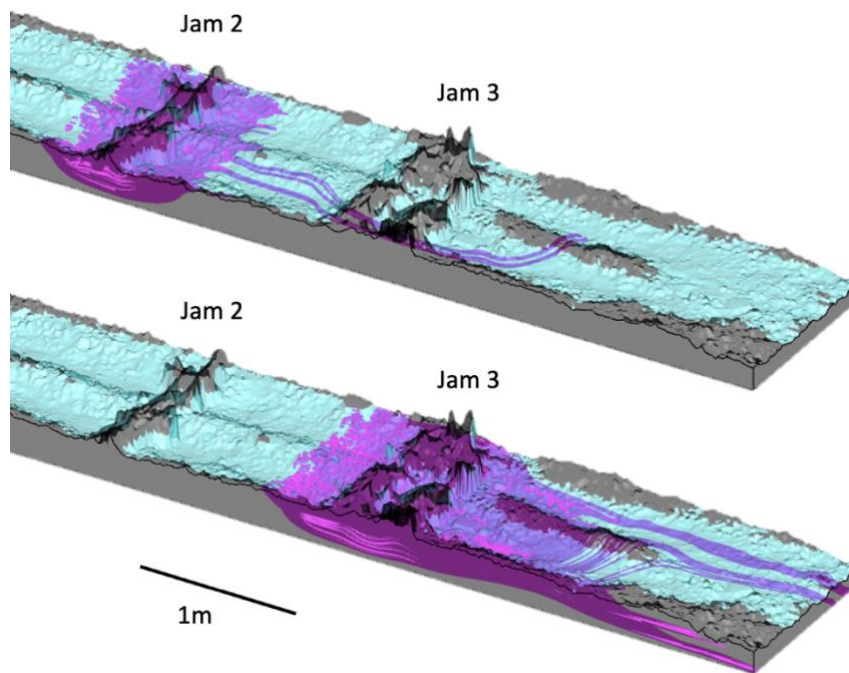


Figure 7. Flow paths (purple) across Jams 2 and 3 for the medium stream discharge. Although the hyporheic flow paths associated with each jam are largely independent of each other, some flow paths that originate at Jam 2 extend downstream and return to the stream below Jam 3 in the gravel bar.

Hyporheic path length distributions (Figure 8) differ substantially in shape as jam volume and complexity increase from Jam 1 to Jam 3. The largest and most complex jam (Jam 3) clearly shows multiple modes of path lengths, indicating the diverse scales of exchange in the presence of both large jam volume and a branched channel. The shortest path lengths at Jam 3 (<0.5m) initiate in the pool immediately upstream and terminate in the jam itself and immediately downstream. Meanwhile, longer path lengths (>0.5m) terminate in the channel farther downstream, including areas along the gravel bar between the channels (Figure 8c). Jam 3 also has the broadest distribution of path lengths (Figure 8c). For example, the difference between the 25th and 90th percentile path lengths at the low-flow condition is 0.59 m for Jam 3, compared to 0.13 m and 0.29 m for Jams 1 and 2, respectively. These distributions shift slightly with stream discharge: as streamflow increases, flow paths become shorter (Figures 8 and 9).

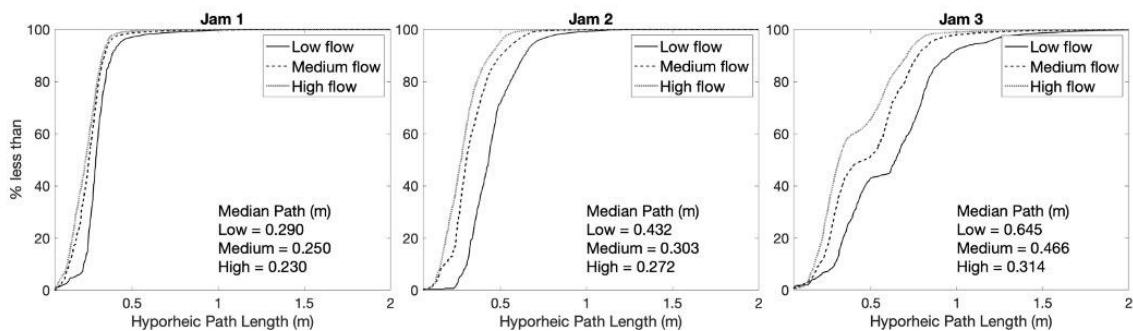


Figure 8. Flux weighted distributions of hyporheic flow path lengths across each jam structure. Jam 1 is farthest upstream within a single channel. Jams 2 and 3 are farther downstream in multi-threaded channel sections.

For a given stream discharge, median path length increases with jam complexity and volume from Jam 1 to Jam 3 (Figures 8 and 9). Larger jams have longer median flow path lengths (50th percentile) and longer extreme flow path lengths (90th percentile) (Figure 9). This suggests that larger jams have a particular capacity to drive long hyporheic flow that spans multiple channel features. Interestingly, the longest lengths appear to be less sensitive to stream flow rate than the median path lengths (compare the range of path lengths across stream flow conditions for the largest jam volume of 0.07 m³ in Figures 9a and 9b). In other words, the longer flows are relatively robust across a range of stream flow conditions. These complex trends show the nonlinear interactions between stream flow rate and the factors that drive hyporheic exchange, which range from hydraulic head gradients to wetted channel extent.

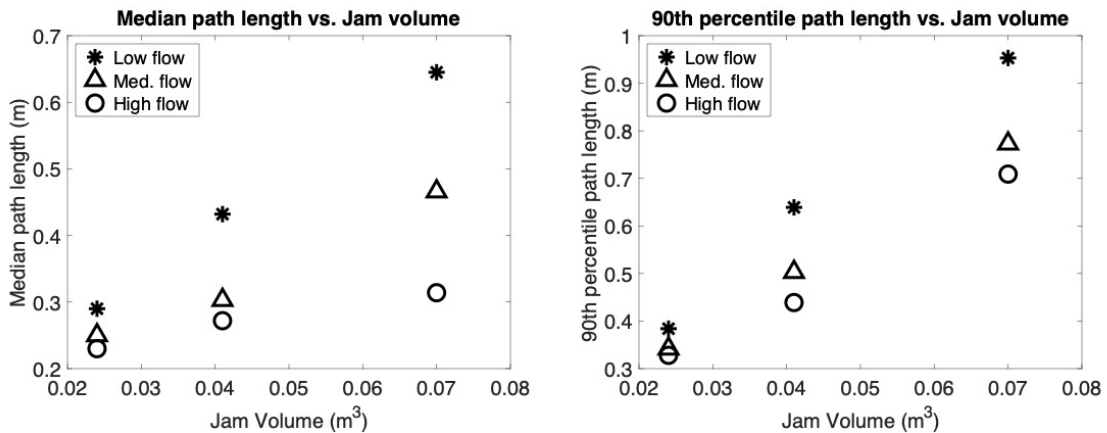


Figure 9. Hyporheic path length increases with jam volume, particularly in the case of the longest flow paths (90th percentile, right).

Hyporheic residence times beneath individual jams generally decrease with increasing stream flow rate, and the distributions for each jam are approximately log-normal (Figure 10), especially for the simpler, smaller upstream jam with a single-threaded channel (Figure 10a). Jams 2 and 3, which are larger and interact with multiple channel threads, have increased ranges of residence times associated with distinct flow path lengths. The faster residence times are associated with shallower flow paths that resurface downstream in the channel closer to the jam structure while the longer residence times are associated with deeper, slower flow paths that migrate farther downstream including through the gravel bar separating the channels.

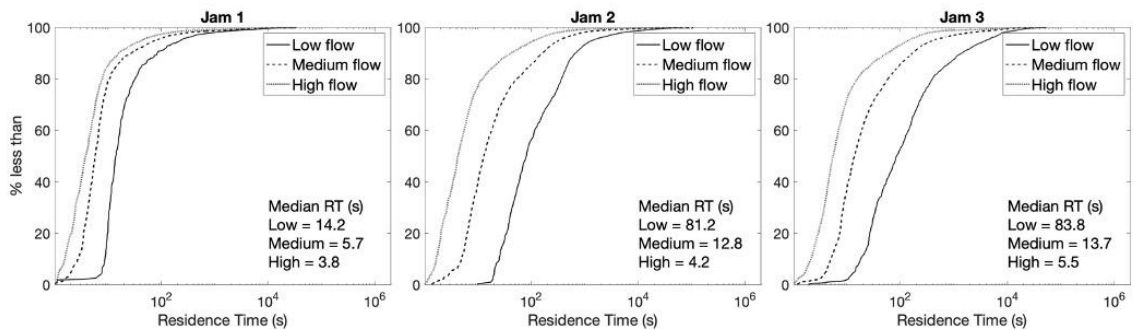


Figure 10. Flux weighted distributions of hyporheic residence times across each jam structure. Jam 1 is upstream, and Jam 3 is downstream (Figure 1).

In model runs without jams, reach-scale hyporheic flow paths are much shorter (Figure 11), and median residence times are generally longer than model runs with jams, especially for greater stream flow conditions (Figure 12). In other words, hyporheic flows

without jams are short and sluggish. Overall, this is consistent with the reduction in exchange fluxes in the absence of jams. The net effect is that the hyporheic zone is more disconnected and acts as more of an immobile zone due to low bed exchange rates.

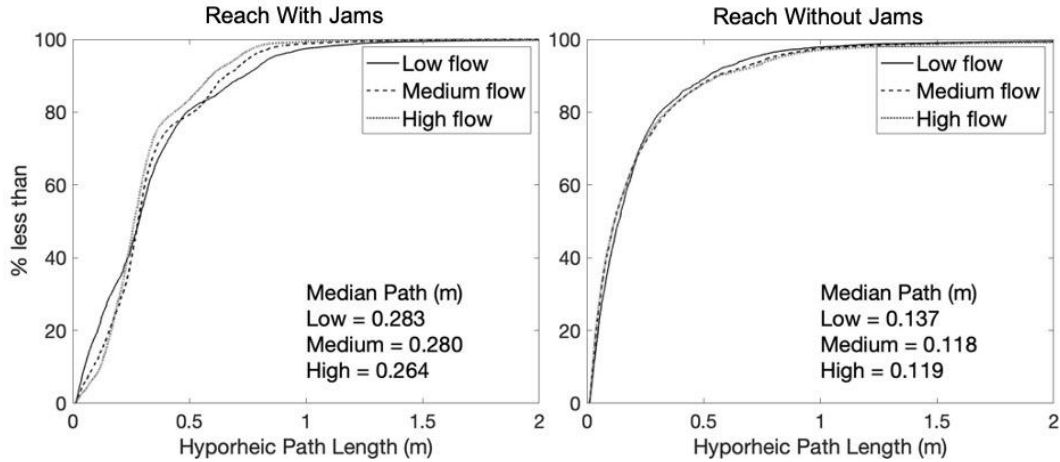


Figure 11. Reach-scale hyporheic path length distributions for model simulations with jams (left) and without jams (right).

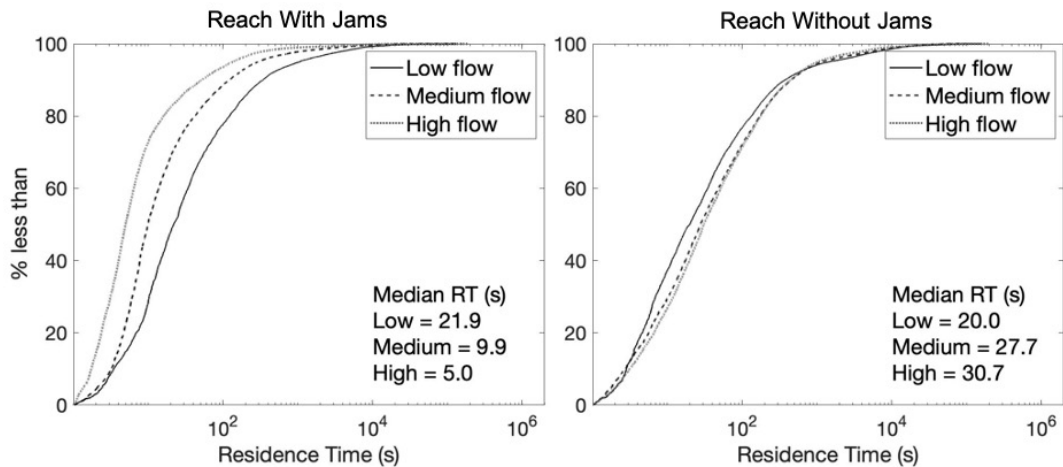


Figure 12. Reach-scale hyporheic residence time distributions for model simulations with jams (left) and without jams (right).

Chapter 4. Discussion

These simulations reveal that: 1) jam structures drive much faster hyporheic exchange, potentially impacting water quality, 2) the combination of large jams and multithreaded channels creates opportunities for hyporheic flow paths that span a wide range of length and time scales.

4.1 Jam Structures Drive Hyporheic Flow and Chemical Reaction Potential in the Hyporheic Zone

My simulations suggest that gravel streams with log jams have much greater hyporheic exchange rates, especially under high stream flow, resulting in more effective turnover. This turnover is due to both the greater wetted streambed area created by backwater effects and the faster fluxes near jams, but particularly the latter. In the flume environment, wetted area only increases by 9-38% when jams are added (depending on stream flow rate), while exchange rates increase by one or more orders of magnitude. Most hyporheic modeling studies do not separate these effects because they are either two-dimensional (Salehin et al., 2004; Cardenas & Wilson, 2007; Sawyer et al., 2011) or three-dimensional with a fixed, predefined wetted area (Cardenas et al., 2004; Doughty et al., 2020; but see Tonina and Buffington (2007) for an exception). While this study suggests that hyporheic fluxes are more responsive than wetted area to changes in jam structure or stream discharge, the behavior may differ in the field, where floodplains can

be extensive and thick vegetation can divert flow from the main channel (Nyssen et al., 2011; Majerova et al., 2015). Majerova et al. (2015) found that less than two years after the establishment of a beaver dam in Curtis Creek in Northern Utah, the total water surface area had more than doubled. Observations of a beaver dam built on top of a log jam during the course of our field measurements at Little Beaver Creek indicate similar increases in backwater storage of water, fine sediment, and particulate organic matter.

Gains in hyporheic connectivity due to jams may have resounding effects on stream water quality. Turnover length and hyporheic residence time together control stream water chemistry, as represented by the reaction significance factor per kilometer, R_s (Harvey and Fuller, 1998):

$$R_s = \frac{\lambda t_{hz} 1000}{L} \quad (9)$$

where λ is reaction rate and t_{hz} is the hyporheic residence time. The reaction significance factor relates the amount of time water spends in the hyporheic zone as it flows downstream with the time required for chemical transformations. Greater values indicate more complete chemical processing over a given reach length (Harvey and Fuller, 1998). The length scale of one kilometer was used in this analysis to compare the experimental flume to a characteristic stream system. In my model trials, simulations with jams had shorter residence times, allowing for less complete chemical processing during a given excursion through the hyporheic zone, but much greater turnover along a reach, allowing for cumulatively more impact on stream water quality, especially at low to medium stream flow rates. For example, assuming a typical reaction rate constant for denitrification in the subsurface of $3 \times 10^{-5} \text{ s}^{-1}$ (0.1 hr^{-1}) (Harvey et al., 2013), the reaction

significance factor per kilometer would range from 0.02-0.07 in my simulations without jams and 0.07-0.35 in my simulations with jams (Figure 13). The effect of jams on reactions such as denitrification (Zarnetske et al., 2011; Harvey et al., 2013) and manganese oxidation (Harvey & Fuller, 1998) is substantial. Reaction significance in the presence of jams is highest at low flow conditions, which is generally when hydrologic retention (t_{hz}/L in Equation 9) is expected to be greatest (Harvey et al., 1996); Morrice et al., 1997). Hydrologic retention has also been shown to scale with frictional resistance (Harvey et al., 2003), which is enhanced by jams and their associated morphologic changes like channel braiding, pools, and riffles. The connection between frictional resistance and hydrologic retention may offer a path forward for predicting the effects of jams on hyporheic processes, but this idea would need to be tested with field experiments.

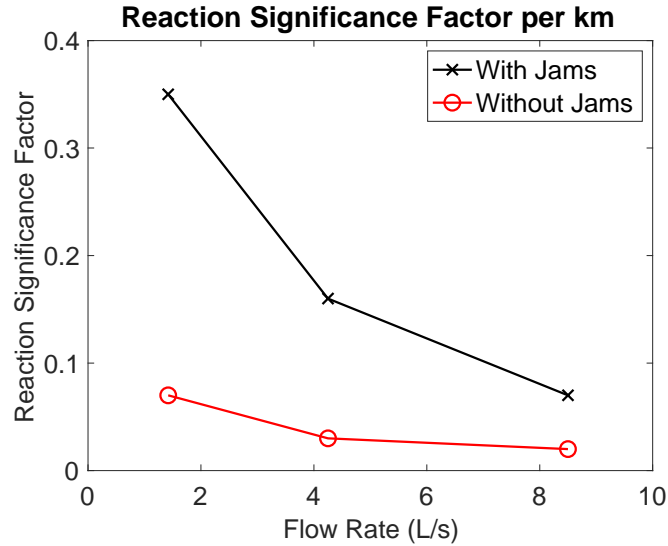


Figure 13: Reaction significance factor per km as a function of stream flow rate for model simulations with and without the presence of jam structures. In this case, the reaction of interest is denitrification.

It is unclear how hyporheic metrics from these flume-scale experiments upscale to the field. In flume experiments and models, Froude numbers were less than 0.1, similar to the field site that inspired the flume experiments, Little Beaver Creek. Sediment and jam permeabilities were likely greater in the flume than many field settings, at least in a scaled sense. However, field-scale estimates of jam permeabilities are generally unknown and are an interesting area for future research. The net result is that specific magnitudes of bed exchange fluxes, hyporheic path lengths, and hyporheic residence times at the field scale cannot be determined from flume-scale experiments, but general qualities (for example, the existence of multiple modes of exchange lengths near more complex jams

and the substantial increase in exchange rates with jams) should be consistent across flume to field scales.

4.2 Multiple Channel Threads and Big Jams Increase Hyporheic Interactions

This study shows that big jams with multiple channel threads encourage multidimensional hyporheic interaction, even for the relatively simple, two-channel system examined here. The flume and model geometry underrepresents the complexities present in anabranching stream systems with jams observed in nature. As jam structures accumulate in a stream channel, upstream pooling increases, driving surface and hyporheic flow paths through the floodplain and aggraded gravel bars, leading to channel avulsion and heightened complexity of the stream system (Mosley, 1981; Abbe & Montgomery, 1996; Sear et al., 2010). Therefore, evolution in channel and jam complexity results in activation of the floodplain and other portions of the hyporheic system that would otherwise be dormant (Morrice et al., 1997; Gooseff et al., 2006; Wondzell et al., 2009; Doughty et al., 2020). Changes in inundation area have been shown to have a profound influence on hyporheic connectivity at field scales on the order of tens of square kilometers (Helton et al., 2014). Future research needs to consider the more complex formation of numerous side channels and flow paths in and around log jams. Models that incorporate greater morphologic complexity and changes in inundation area should reveal even greater influence of jams on multidimensional hyporheic flows.

Comparing the second and third jams in the flume, it also appears that larger jams are particularly effective at initiating longer hyporheic flow paths and can promote multiple dominant exchange length scales and residence times. The multimodal path lengths and wide distribution of residence times across the largest jam structure (Jam 3) may explain the field observations of Doughty et al. (2020) in which bimodal solute breakthrough was measured downstream of a large jam. Larger jams also have the ability to generate increased upstream pooling and alter stream energy gradients, as detailed by Faustini and Jones (2003). It is important to ask what is more important for hyporheic connectivity—jam volume or frequency. Mutz et al. (2007) found that a fairly even distribution of many small wood pieces across a flume channel increased the flux, volume, and depth of the active hyporheic zone. They did not test the effects of uneven jam-like distributions. Dudunake et al. (2020) observed a similar increase in exchange around many relatively evenly-spaced boulders in a flume. The structure of wood pieces and their orientation and grouping are likely to have a wide range of effects on wetted channel area and pooling upstream of jams that I am unable to test with my jam representation in the current model framework. Successful application of stream management plans utilizing log jams is dependent upon understanding the hyporheic effects of different large wood distributions (ranging from more dispersed distributions to many smaller, successional jam structures to fewer, larger jams).

Chapter 5. Conclusion

The presence of log jam structures increases channel wetted area and bed hyporheic exchange flux, particularly the latter, driving longer subsurface flow paths that connect multiple jam structures. Jams facilitate more opportunities for solute retention and processing in the hyporheic zone, especially at lower flow rates, when hydrologic retention peaks. This study further highlights the influence that larger log jams in combination with multiple channel branches have on hyporheic systems, namely increased ranges of hyporheic length and time scales. The resulting effects of these jam-induced hyporheic patterns on chemical processes, measured by the reaction significance factor, emphasizes the value of log jams on overall stream function. Areas for further research include determining how jam frequency and the properties of individual jams (permeability and porosity) influence the co-evolution of channel morphology and hyporheic flow in forested streams.

Bibliography

- Abbe, T.B. and Montgomery, D.R. (1996), Large woody debris jams, channel hydraulics, and habitat formation in large rivers. *Regul. Rivers: Res. Mgmt.*, 12: 201-221. [https://doi-org.proxy.lib.ohio-state.edu/10.1002/\(SICD\)1099-1646\(199603\)12:2/3<201::AID-RRR390>3.0.CO;2-A](https://doi-org.proxy.lib.ohio-state.edu/10.1002/(SICD)1099-1646(199603)12:2/3<201::AID-RRR390>3.0.CO;2-A)
- Ader, E., Wohl, E., McFadden, S., & Singha, K. (2021). Logjams as a driver of transient storage in a mountain stream. *Earth Surface Processes and Landforms*, 46(3), 701–711. <https://doi.org/10.1002/esp.5057>
- Arrigoni, A. S., Poole, G. C., Mertes, L. A. K., O’Daniel, S. J., Woessner, W. W., & Thomas, S. A. (2008). Buffered, lagged, or cooled? Disentangling hyporheic influences on temperature cycles in stream channels. *Water Resources Research*, 44(9). <https://doi.org/10.1029/2007WR006480>
- Bear, J. (1972). Dynamics of fluids in porous media, American Elsevier, New York, NY.
- Beckman, N. D., & Wohl, E. (2014). Carbon storage in mountainous headwater streams: The role of old-growth forest and logjams. *Water Resources Research*, 50(3), 2376–2393. <https://doi.org/10.1002/2013WR014167>
- Buffington, J. M., & Tonina, D. (2009). Hyporheic Exchange in Mountain Rivers II: Effects of Channel Morphology on Mechanics, Scales, and Rates of Exchange. *Geography Compass*, 3(3), 1038–1062. <https://doi.org/10.1111/j.1749-8198.2009.00225.x>
- Cardenas, M. B., Wilson, J. L., & Zlotnik, V. A. (2004). Impact of heterogeneity, bed forms, and stream curvature on subchannel hyporheic exchange: MODELING STUDY OF HYPORHEIC EXCHANGE. *Water Resources Research*, 40(8). <https://doi.org/10.1029/2004WR003008>
- Chow, R., Wu, H., Bennett, J. P., Dugge, J., Wöhling, T., & Nowak, W. (2019). Sensitivity of Simulated Hyporheic Exchange to River Bathymetry: The Steinlach River Test Site. *Groundwater*, 57(3), 378–391. <https://doi.org/10.1111/gwat.12816>
- Collins, B. D., Montgomery, D. R., Fetherston, K. L., & Abbe, T. B. (2012). The floodplain large-wood cycle hypothesis: A mechanism for the physical and biotic structuring of temperate forested alluvial valleys in the North Pacific coastal ecoregion. *Geomorphology*, 139–140, 460–470. <https://doi.org/10.1016/j.geomorph.2011.11.011>
- Crenshaw, C. L., Valett, H. M., & Webster, J. R. (2002). Effects of augmentation of coarse particulate organic matter on metabolism and nutrient retention in hyporheic sediments. *Freshwater Biology*, 47(10), 1820–1831. <https://doi.org/10.1046/j.1365-2427.2002.00928.x>

- Curran, J. H., & Wohl, E. E. (2003). Large woody debris and flow resistance in step-pool channels, Cascade Range, Washington. *Geomorphology*, 51(1), 141–157. [https://doi.org/10.1016/S0169-555X\(02\)00333-1](https://doi.org/10.1016/S0169-555X(02)00333-1)
- Dolzyk, K., & Chmielewska, I. (2014). Predicting the Coefficient of Permeability of Non-Plastic Soils. *Soil Mechanics and Foundation Engineering*, 51(5), 213–218. <https://doi.org/10.1007/s11204-014-9279-3>
- Doughty, M., Sawyer, A. H., Wohl, E., & Singha, K. (2020). Mapping increases in hyporheic exchange from channel-spanning logjams. *Journal of Hydrology*, 587, 124931. <https://doi.org/10.1016/j.jhydrol.2020.124931>
- Dudunake, T., Tonina, D., Reeder, W. J., & Monsalve, A. (2020). Local and Reach-Scale Hyporheic Flow Response From Boulder-Induced Geomorphic Changes. *Water Resources Research*, 56(10), e2020WR027719. <https://doi.org/10.1029/2020WR027719>
- El-Kadi, A. I., & Ling, G. (1993). The Courant and Peclet Number criteria for the numerical solution of the Richards Equation. *Water Resources Research*, 29(10), 3485–3494. <https://doi.org/10.1029/93WR00929>
- Elder, J. W. (1959). The dispersion of marked fluid in turbulent shear flow. *Journal of Fluid Mechanics*, 5(04), 544. <https://doi.org/10.1017/S0022112059000374>
- Endreny, T., Lautz, L., & Siegel, D. I. (2011). Hyporheic flow path response to hydraulic jumps at river steps: Flume and hydrodynamic models. *Water Resources Research*, 47(2). <https://doi.org/10.1029/2009WR008631>
- Evans, E. C., & Petts, G. E. (1997). Hyporheic temperature patterns within riffles. *Hydrological Sciences Journal*, 42(2), 199–213. <https://doi.org/10.1080/02626669709492020>
- Faustini, J. M., & Jones, J. A. (2003). Influence of large woody debris on channel morphology and dynamics in steep, boulder-rich mountain streams, western Cascades, Oregon. *Geomorphology*, 51(1), 187–205. [https://doi.org/10.1016/S0169-555X\(02\)00336-7](https://doi.org/10.1016/S0169-555X(02)00336-7)
- Fischer, H. B. (1965). Discussion of “numerical solution to a dispersion equation.” *Journal of the Hydraulics Division*, 91(2), 402–407. <https://doi.org/10.1061/JYCEAJ.0001226>
- Fischer, H. B. (1968). Methods for predicting dispersion coefficients in natural streams: with applications to lower reaches of the Green and Duwamish Rivers, Washington (Ser. Dispersion in surface water). U.S. Govt. Print. Off.
- Gandy, C. J., Smith, J. W. N., & Jarvis, A. P. (2007). Attenuation of mining-derived pollutants in the hyporheic zone: A review. *Science of The Total Environment*, 373(2), 435–446. <https://doi.org/10.1016/j.scitotenv.2006.11.004>
- Glover, R. E. (1964). Dispersion of dissolved or suspended materials in flowing streams (Ser. Geological survey. professional paper, 433-b). U.S. Gov. Print. Off.
- Gooseff, M. N., Anderson, J. K., Wondzell, S. M., LaNier, J., & Haggerty, R. (2006). A modelling study of hyporheic exchange pattern and the sequence, size, and spacing of stream bedforms in mountain stream networks, Oregon, USA. *Hydrological Processes*, 20(11), 2443–2457. <https://doi.org/10.1002/hyp.6349>

- Guggenheim, E. A. (1954). The diffusion coefficient of sodium chloride. *Transactions of the Faraday Society*, 50, 1048–1048. <https://doi.org/10.1039/tf9545001048>
- Harvey, J. W., Wagner, B. J., & Bencala, K. E. (1996). Evaluating the Reliability of the Stream Tracer Approach to Characterize Stream-Subsurface Water Exchange. *Water Resources Research*, 32(8), 2441–2451. <https://doi.org/10.1029/96WR01268>
- Harvey, J. W., & Fuller, C. C. (1998). Effect of enhanced manganese oxidation in the hyporheic zone on basin-scale geochemical mass balance. *Water Resources Research*, 34(4), 623–636. <https://doi.org/10.1029/97WR03606>
- Harvey, J. W., & Wagner, B. J. (2000). Quantifying Hydrologic Interactions between Streams and Their Subsurface Hyporheic Zones. In *Streams and Ground Waters* (pp. 3–44). Elsevier. <https://doi.org/10.1016/B978-012389845-6/50002-8>
- Harvey, J. W., Conklin, M. H., & Koelsch, R. S. (2003). Predicting changes in hydrologic retention in an evolving semi-arid alluvial stream. *Advances in Water Resources*, 26(9), 939–950. [https://doi.org/10.1016/S0309-1708\(03\)00085-X](https://doi.org/10.1016/S0309-1708(03)00085-X)
- Harvey, J. W., Böhlke, J. K., Voytek, M. A., Scott, D., & Tobias, C. R. (2013). Hyporheic zone denitrification: Controls on effective reaction depth and contribution to whole-stream mass balance. *Water Resources Research*, 49(10), 6298–6316. [https://doi.org/10.1002/wrcr.20492@10.1002/\(ISSN\)1944-7973.AQUIDER1](https://doi.org/10.1002/wrcr.20492@10.1002/(ISSN)1944-7973.AQUIDER1)
- Helton, A. M., Poole, G. C., Payn, R. A., Izurieta, C., & Stanford, J. A. (2014). Relative influences of the river channel, floodplain surface, and alluvial aquifer on simulated hydrologic residence time in a montane river floodplain. *Geomorphology*, 205, 17–26. <https://doi.org/10.1016/j.geomorph.2012.01.004>
- Hester, E. T., & Gooseff, M. N. (2010). Moving Beyond the Banks: Hyporheic Restoration Is Fundamental to Restoring Ecological Services and Functions of Streams. *Environmental Science & Technology*, 44(5), 1521–1525. <https://doi.org/10.1021/es902988n>
- Huyakorn, P. S., Springer, E. P., Guvanasen, V., & Wadsworth, T. D. (1986). A three-dimensional finite-element model for simulating water flow in variably saturated porous media. *Water Resources Research*, 22(13), 1790–1808. <https://doi.org/10.1029/WR022i013p01790>
- Jaiswal, S., Chopra, M., & Das, S. (2018). Numerical Solution of Two-Dimensional Solute Transport System Using Operational Matrices. *Transport in Porous Media*, 122(1), 1–23. <https://doi.org/10.1007/s11242-017-0986-x>
- Lautz, L. K., Siegel, D. I., & Bauer, R. L. (2006). Impact of debris dams on hyporheic interaction along a semi-arid stream. *Hydrological Processes*, 20(1), 183–196. <https://doi.org/10.1002/hyp.5910>
- Livers, B., & Wohl, E. (2016). Sources and interpretation of channel complexity in forested subalpine streams of the Southern Rocky Mountains: CHANNEL COMPLEXITY IN FORESTED STREAMS. *Water Resources Research*, 52(5), 3910–3929. <https://doi.org/10.1002/2015WR018306>
- Majerova, M., Neilson, B. T., Schmadel, N. M., Wheaton, J. M., & Snow, C. J. (2015). Impacts of beaver dams on hydrologic and temperature regimes in a mountain stream. *Hydrology and Earth System Sciences*, 19(8), 3541–3556. <https://doi.org/10.5194/hess-19-3541-2015>

- Massong, T. M., & Montgomery, D. R. (2000). Influence of sediment supply, lithology, and wood debris on the distribution of bedrock and alluvial channels. *The Geological Society of America Bulletin*, 112(4), 591–591.
- Montgomery, D. R., Massong, T. M., & Hawley, S. C. S. (2003). Influence of debris flows and log jams on the location of pools and alluvial channel reaches, Oregon Coast Range. *GSA Bulletin*, 115(1), 78–88. [https://doi.org/10.1130/0016-7606\(2003\)115<0078:IODFAL>2.0.CO;2](https://doi.org/10.1130/0016-7606(2003)115<0078:IODFAL>2.0.CO;2)
- Montgomery, D. R., & Buffington, J. M. (1997). Channel-reach morphology in mountain drainage basins. *The Geological Society of America Bulletin*, 109(5), 596.
- Morrice, J. A., Valett, H. M., Dahm, C. N., & Campana, M. E. (1997). Alluvial Characteristics, groundwater-surface water exchange and hydrological retention in headwater streams. *Hydrological Processes*, 11, 253–267.
- Mosley, M. P. (1981). The influence of organic debris on channel morphology and bedload transport in a New Zealand forest stream. *Earth Surface Processes and Landforms*, 6(6), 571–579. <https://doi.org/10.1002/esp.3290060606>
- Mutz, M., Kalbus, E., & Meinecke, S. (2007). Effect of instream wood on vertical water flux in low-energy sand bed flume experiments. *Water Resources Research*, 43(10). <https://doi.org/10.1029/2006WR005676>
- Newbold, J. D., Elwood, J. W., O'Neill, R. V., & Sheldon, A. L. (1983). Phosphorus Dynamics in a Woodland Stream Ecosystem: A Study of Nutrient Spiralling. *Ecology*, 64(5), 1249–1265. <https://doi.org/10.2307/1937833>
- Nyssen, J., Pontzele, J., & Billi, P. (2011). Effect of beaver dams on the hydrology of small mountain streams: Example from the Cheval in the Ourthe Orientale basin, Ardennes, Belgium. *Journal of Hydrology*, 402(1), 92–102. <https://doi.org/10.1016/j.jhydrol.2011.03.008>
- Panday, S., Huyakorn, P. S., Therrien, R., & Nichols, R. L. (1993). Improved three-dimensional finite-element techniques for field simulation of variably saturated flow and transport. *Journal of Contaminant Hydrology*, 12(1–2), 3–33. [https://doi.org/10.1016/0169-7722\(93\)90013-I](https://doi.org/10.1016/0169-7722(93)90013-I)
- Phillips, J. V., Tadayon, S., Flood Control District of Maricopa County, & Geological Survey (U.S.). (2006). *Selection of manning's roughness coefficient for natural and constructed vegetated and non-vegetated channels, and vegetation maintenance plan guidelines for vegetated channels in Central Arizona* (Ser. Scientific investigations report, 2006-5108). U.S. Dept. of the Interior, U.S. Geological Survey
- Salehin, M., Packman, A. I., & Paradis, M. (2004). Hyporheic exchange with heterogeneous streambeds: Laboratory experiments and modeling. *Water Resources Research*, 40(11). <https://doi.org/10.1029/2003WR002567>
- Savant, S. A., Reible, D. D., & Thibodeaux, L. J. (1987). Convective transport within stable river sediments. *Water Resources Research*, 23(9), 1763–1768. <https://doi.org/10.1029/WR023i009p01763>
- Sawyer, A. H., Cardenas, M. B., & Buttle, J. (2011). Hyporheic exchange due to channel-spanning logs. *Water Resources Research*, 47(8). <https://doi.org/10.1029/2011WR010484>

- Sear, D. A., Millington, C. E., Kitts, D. R., & Jeffries, R. (2010). Logjam controls on channel: Floodplain interactions in wooded catchments and their role in the formation of multi-channel patterns. *Geomorphology*, 116(3), 305–319. <https://doi.org/10.1016/j.geomorph.2009.11.022>
- Shahabi, A. A., Das, B. M. & Tarquin, A. J. (1984). *Empirical relation for coefficient of permeability of sand*, National Conference Publication, Institution of Engineers, Australia, 84, No. 2, 54-57.
- Spreitzer, G., Tunnicliffe, J., & Friedrich, H. (2020). Porosity and volume assessments of large wood (LW) accumulations. *Geomorphology*, 358, 107122. <https://doi.org/10.1016/j.geomorph.2020.107122>
- Therrien, R., 1992. Three-dimensional analysis of variably-saturated flow and solute transport in discretely-fractured porous media. Ph.D. Thesis, University of Waterloo, Waterloo, Ont.
- Therrien, R., & Sudicky, E. A. (1996). Three-dimensional analysis of variably-saturated flow and solute transport in discretely-fractured porous media. *Journal of Contaminant Hydrology*, 23(1–2), 1–44. [https://doi.org/10.1016/0169-7722\(95\)00088-7](https://doi.org/10.1016/0169-7722(95)00088-7)
- Tonina, D., & Buffington, J. M. (2007). Hyporheic exchange in gravel bed rivers with pool-riffle morphology: Laboratory experiments and three-dimensional modeling. *Water Resources Research*, 43(1). <https://doi.org/10.1029/2005WR004328>
- Tonina, D., & Buffington, J. M. (2009). Hyporheic Exchange in Mountain Rivers I: Mechanics and Environmental Effects. *Geography Compass*, 3(3), 1063–1086. <https://doi.org/10.1111/j.1749-8198.2009.00226.x>
- Valett, H. M., Dahm, C. N., Campana, M. E., Morrice, J. A., Baker, M. A., & Fellows, C. S. (1997). Hydrologic Influences on Groundwater-Surface Water Ecotones: Heterogeneity in Nutrient Composition and Retention. *Journal of the North American Benthological Society*, 16(1), 239–247. <https://doi.org/10.2307/1468254>
- Ventres-Pake, R., Nahorniak, M., Kramer, N., O’Neal, J., & Abbe, T. (2020). Integrating Large Wood Jams into Hydraulic Models: Evaluating a Porous Plate Modeling Method. *JAWRA Journal of the American Water Resources Association*, 56(2), 333–347. <https://doi.org/10.1111/1752-1688.12818>
- Wondzell, S. M., LaNier, J., Haggerty, R., Woodsmith, R. D., & Edwards, R. T. (2009). Changes in hyporheic exchange flow following experimental wood removal in a small, low-gradient stream. *Water Resources Research*, 45(5). <https://doi.org/10.1029/2008WR007214>
- Xu, M., Wang, Z., Pan, B., & Zhao, N. (2012). Distribution and species composition of macroinvertebrates in the hyporheic zone of bed sediment. *International Journal of Sediment Research*, 27(2), 129–140. [https://doi.org/10.1016/S1001-6279\(12\)60022-5](https://doi.org/10.1016/S1001-6279(12)60022-5)
- Xu, Y., & Liu, X. (2017). Effects of Different In-Stream Structure Representations in Computational Fluid Dynamics Models—Taking Engineered Log Jams (ELJ) as an Example. *Water*, 9(2), 110. <https://doi.org/10.3390/w9020110>
- Zarnetske, J. P., Haggerty, R., Wondzell, S. M., & Baker, M. A. (2011). Dynamics of nitrate production and removal as a function of residence time in the hyporheic zone.

Journal of Geophysical Research, 116(G1), G01025.

<https://doi.org/10.1029/2010JG001356>

Zhu, J., & Mohanty, B. P. (2002). Spatial Averaging of van Genuchten Hydraulic Parameters for Steady-State Flow in Heterogeneous Soils: A Numerical Study. *VADOSE ZONE J.*, 1, 12.

Appendix A. Model Development and HydroGeoSphere Input Files

Necessary Software and Model Setup

Necessary software (function):

- Agisoft (photogrammetry)
- ArcMap and/or QGIS (geospatial)
- AlgoMesh (grid development)
- HydroGeoSphere (model execution)
- Tecplot (model visualization)
- MATLAB and Python (Tecplot integration and data post-processing)

General steps to model generation:

1. Photograph flume
2. Build digital elevation model (DEM) from flume photos using Agisoft
3. Process DEM and model features (zones and boundary conditions) in ArcMap and/or QGIS
4. Construct model grid mesh and specify feature elements and nodes in AlgoMesh
5. Build HydroGeoSphere input files (see below) and run models
6. Visualize model outputs, bed exchange fluxes, and conduct particle tracking analysis in Tecplot
7. Process hyporheic residence time and path length distributions

Model Input File - Medium Flow Condition

Note: This input file was used for simulating coupled surface and subsurface flow for the medium-discharge scenario. It uses output files from a ramp-up simulation that only solves for surface flow with an impermeable bed.

```
!----- Problem description
Flume Model (Med. Flow)
end title

!-----Grid generation

read algomesh 2d grid
    ./mesh/Flume_DEM_2cm.ah2

generate layers interactive
```

```

zone by layer

base elevation

    elevation from raster file
    ./mesh/BaseLayer.asc

end

new layer
    layer name
    Mid Layer

    uniform sublayering
    7

    elevation from raster file
    ./mesh/FinalDEM_NoJams_final.asc

    offset top
    0.496667 !0.07+0.426667 (layer thickness + minimum
elevation from DEM raster file)
end

new layer
    layer name
    Top layer

    uniform sublayering
    3

    elevation from raster file
    ./mesh/FinalDEM_Jams234_final.asc

    offset top
    0.508443 !0.07(from above)+0.03+0.408443 (deeper layer
thickness + layer thickness + minimum elevation from DEM raster
file)

end

end !generate layers interactive

end grid generation

!----- General simulation parameters
units: kilogram-metre-second
transient flow
unsaturated
dual nodes for surface flow

```

```

!-----Porous media properties

use domain type
porous media

properties file
flume.mprops

!-----Set sediment properties

!--deep sediments
clear chosen zones
clear chosen elements
choose elements am
./mesh/Jams234_ModelExtent.echos
1,5          !Five deepest porous media layers
new zone
1
choose zone number
1
read properties
sediments_deep

!--shallow sediments
clear chosen zones
clear chosen elements
choose elements am
./mesh/Jams234_ModelExtent.echos
6,11        !Shallow porous media layers (pattern continues below)

!--Shallow sediments under jam
choose elements am
./mesh/Jams234_Jam2.echos
6,8
choose elements am
./mesh/Jams234_Jam3.echos
6,8
choose elements am
./mesh/Jams234_Jam4.echos
6,8
!----
new zone
2
choose zone number
2
read properties
sediments_shallow

!--Reach 2 Jam
clear chosen zones

```

```

clear chosen elements
choose elements am
./mesh/Jams234_Jam2.echos
8,11
new zone
3
choose zone number
3
read properties
log_jam

!---Reach 3 Jams
clear chosen zones
clear chosen elements
choose elements am
./mesh/Jams234_Jam3.echos
8,11
new zone
4
choose zone number
4
read properties
log_jam

!---Reach 4 Jam
clear chosen zones
clear chosen elements
choose elements am
./mesh/Jams234_Jam4.echos
8,11
new zone
5
choose zone number
5
read properties
log_jam

!-----overland flow properties
use domain type
surface

properties file
flume.oprops

clear chosen faces
choose faces top

new zone
1

clear chosen zones

```

```
choose zone number
1
read properties
overland flow

!--Jam 2 zone
clear chosen faces
choose faces top am
./mesh/Jams234_Jam2.echos

new zone
2

clear chosen zones
choose zone number
2
read properties
overland flow

!--Jam 3 zone
clear chosen faces
choose faces top am
./mesh/Jams234_Jam3.echos

new zone
3

clear chosen zones
choose zone number
3
read properties
overland flow

!--Jam 4 zone
clear chosen faces
choose faces top am
./mesh/Jams234_Jam4.echos

new zone
4

clear chosen zones
choose zone number
4
read properties
overland flow

!-----boundary conditions
use domain type
porous media
```

```

initial head from output file
./InitConds/flume_medflow_feb2021o.head_pm.0001      !previous sim.

use domain type
surface

initial head from output file
./InitConds/flume_medflow_feb2021o.head_olf.0001    ! previous sim.

!--Inlet
clear chosen nodes
choose nodes top am
./mesh/Jams234_Inlet.nchos

create node set
inlet

boundary condition
  type
  flux nodal

  node set
  inlet

  time value table
  0.0 0.000047222      !0.00425/90nodes (medium flow = 4.25L/s)
  end

  tecplot output

end

!--Outlet - surface
clear chosen nodes
choose nodes top am
./mesh/Jams234_Outlet.nchos

create segment set
outlet

boundary condition
  type
  critical depth

  name
  CritDepth_outlet

  segment set
  outlet

  tecplot output

```

```

end

!--Outlet - subsurface
use domain type
porous media

clear chosen nodes
choose nodes am
./mesh/Jams234_Outlet.nchos
1,11

create face set
subdrain

boundary condition
    type
    free drainage

    face set
    subdrain

end

!----- convergence criteria
Jacobian epsilon
1.0d-5
Newton absolute convergence criteria
1.0d-5
Newton residual convergence criteria
5.4d-4

!----- Timestep controls
saturation control
0.050

initial time
345600.0      !4 days

initial timestep
0.125
maximum timestep multiplier
2.5
minimum timestep multiplier
0.5

output times
1400000.0
end

```

Porous Media Properties Input File

```
!-----sediments_deep properties
sediments_deep

K isotropic
0.000889

porosity
0.30

longitudinal dispersivity
0.05

transverse dispersivity
0.005

vertical transverse dispersivity
0.005

unsaturated van genuchten functions
  residual saturation
    0.053 !default HGS value = 0.053; ref pg. 203
  alpha
    3.548 !for sands, Zhu and Mohanty, 2002
  beta
    3.162 !for sands, Zhu and Mohanty, 2002
end

end material

!-----sediments_shallow properties
sediments_shallow

K isotropic
0.0254

porosity
0.30

longitudinal dispersivity
0.05

transverse dispersivity
0.005

vertical transverse dispersivity
0.005

unsaturated van genuchten functions
  residual saturation
```

```
        0.053    !default HGS value = 0.053; ref pg. 203
    alpha
        3.548    !for sands, Zhu and Mohanty, 2002
    beta
        3.162    !for sands, Zhu and Mohanty, 2002
end

end material

!-----jam properties
log_jam

K isotropic
1.0

porosity
0.70

longitudinal dispersivity
1.4

transverse dispersivity
1.4

end material
```

Surface Flow Properties Input File

```
overland flow

X friction
0.030

Y friction
0.030

longitudinal dispersivity
1.4

transverse dispersivity
1.4

end material
```